ADVANCED FUNCTIONAL MATERIALS
www.afm-journal.de

Flexible Janus Nanoribbons Array: A New Strategy to Achieve Excellent Electrically Conductive Anisotropy, Magnetism, and Photoluminescence

Qianli Ma, Jinxian Wang, Xiangting Dong, Wensheng Yu, and Guixia Liu*

A new type of flexible Janus nanoribbons array with anisotropic electrical conductivity, magnetism, and photoluminescence has been successfully fabricated by electrospinning technology using a specially designed parallel spinneret. Every single Janus nanoribbon in the array consists of a half side of Fe_3O_4 nanoparticles/polyaniline/polymethylmethacrylate (PMMA) conductive-magnetic bifunctionality and the other half side of $Tb(BA)_3$phen/PMMA insulative-photoluminescent characteristics, and all the Janus nanoribbons are aligned to form array. Owing to the unique nanostructure, the conductance along with the length direction of nanoribbons reaches up to eight orders of magnitude higher than that along with perpendicular direction, which is by far the most excellent conductive anisotropy for anisotropic conductive materials. The Janus nanoribbons array is also simultaneously endowed with magnetic and photoluminescent characteristics. The obtained Janus nanoribbons array will have important applications in the future subminiature electronic equipments owing to its high electrical anisotropy and multifunctionality. Furthermore, the design concept and fabrication technique for the flexible Janus nanoribbons array provide a new and facile approach for the preparation of anisotropic conductive films with multifunctionality.

1. Introduction

At present, electronic components are developing toward the direction of smaller, lighter, higher number of I/O (Input/Output), and higher performance. With advances in electronic packaging technology, it requires that the electronic system not only has high performance but also is low cost. Therefore, it is an urgent need to develop new types of interconnected materials. Anisotropic conductive films (ACFs) have been widely used as one kind of green materials in electronic packaging owing to their many advantages: (1) high density connection in narrow space achievable; (2) insulative in needless directions (so that the short circuit can be prevented), etc. ACFs can be divided into two types according to their conducting direction. The first type of ACFs is conductive along the direction of the thicknesses of the films and insulative along their surfaces (we name them as type I ACFs for convenience).[1–5] This type of ACFs has been widely applied in the production of electronic devices and mature techniques from production to application for them already exist. The second type of ACFs has different conductivities along with different directions of their surfaces (we name them as type II ACFs, the focus of this study). Especially, the researchers have been spending a great deal of efforts to achieve the type II ACFs which are conductive along one direction and insulative along the others. Typically, type II ACF is a single or multilayer thin film material that comprehends parallel-arranged 1D conductive units, such as chains or nanofibers, and these 1D conductive units are separated from each other with air and/or interfaces (act as the resistors).[6–8] The direction of the length of these 1D conductive units is denoted as X direction and the direction that is perpendicular to X along the film surface is denoted as Y direction. Thus, of the type II ACFs, the electrical conduction along with X direction is higher than that along Y direction due to different electrical connection in the two directions. Up to now, some kinds of type II ACFs have been fabricated. Jeon et al.[9] studied the optical and electrical properties of preferentially anisotropic single-walled carbon-nanotube films. The carbon nanotube network is composed of metallic and semiconducting nanotubes embedded in an air dielectric host, and the electrical properties are different along X and Y directions. Ra et al.[10] synthesized the multiwalled carbon nanotubes (MWCNTs) embedded polyacrylonitrile nanofiber paper via electrospinning, and its conductivity along X direction is three times higher than that along Y direction. Majewski et al.[11] achieved anisotropic ionic conductivity in block copolymer membranes by magnetic field alignment. The conductivity along X direction of the membranes reaches up to 1000 times higher than Y direction. Very recently, Huang et al.[12] fabricated an

Dr. Q. Ma, Prof. J. Wang, Prof. X. Dong, Dr. W. Yu, Prof. G. Liu
Key Laboratory of Applied Chemistry and Nanotechnology at Universities of Jilin Province
Changchun University of Science and Technology
Changchun 130022, P.R. China
E-mail: dongxiangting888@163.com

DOI: 10.1002/adfm.201500348

anisotropic conductive polymer film by shear-flow inducing MWCNTs to be assembled into well-ordered parallel MWCNT stripes vertical to the shear flow. The electrical measurement showed that the electrical resistivity along the MWCNT stripes was 6 orders of magnitude lower than that orthogonal to the stripes, which was the reported most striking conductive anisotropy for the plastic anisotropic conductive materials.

However, at this stage, breakthroughs of type II ACFs are in lab-only, with no solution yet for industrial applications due to their some unsolved defects: First, some kinds of type II ACFs are quite brittle, resulting in the poor deformation, bending, and stretching ability; second, the sizes of some type II ACFs are very small (even less than 1×1 cm^2) due to the limitation of preparation methods; third, the type II ACFs that are composed of various fibers arrays usually do not have high conductivity ratio between X and Y directions (mostly lower than 1000 times), leading to insufficient conductivity along X direction or poor insulativity along Y direction; fourth, some preparation methods for the type II ACFs require multistep and high precision, resulting in high cost and low yield. All of these defects limit the practical applications of the type II ACFs.

Electrospinning technique has been widely adopted to effectively fabricate 1D nanomaterials and has been applied in many areas such as filtration,[13] optical and chemical sensors,[14] biological scaffolds,[15] electrode materials,[16] luminescent materials, and [17] photocatalysts.[18,19] The electrospun products have some unique advantages, such as long length (up to several meters), good flexibility (owing to the polymer template), and low-power consumption. The electrospun products can also be arranged as arrays by using special collectors.[20–24] Not long ago, we have fabricated a new-typed nanoribbon with asymmetric dual-sided structure via electrospinning, which is named as Janus (a Roman god with two faces) nanoribbon.[25] Janus nanoribbon consists of two different sides assembled side-by-side, thus an asymmetric integration of different functions is realized. In this study, we use this Janus nanoribbon structure to successfully acquire a new kind of type II ACF via electrospinning technique. Here, one side of a Janus nanoribbon is composed of Fe_3O_4/polyaniline (PANI)/polymethylmethacrylate (PMMA) (conductive-magnetic side) and the other side consists of $Tb(BA)_3$phen/PMMA (insulative-photoluminescent side). All the Janus nanoribbons are arranged in the same direction by using a rolling aluminum rotary drum as the collector. Thus it is expected that the resultant [Fe_3O_4/PANI/PMMA]//[$Tb(BA)_3$phen/PMMA] Janus nanoribbons array will possess high electrically conductive ratio between its X and Y directions owing to introducing of insulative sides. Furthermore, the Janus nanoribbons array is also simultaneously endowed with magnetic and photoluminescent characteristics to achieve multifunctionality. The structure, conductivity, photoluminescence, and magnetism of the Janus nanoribbons array were systematically investigated and some new results were obtained. The Janus nanoribbons array overcomes the above-mentioned defects of the existing type II ACFs, which will have important applications in high density electrical connection in narrow space, such as in mobile phones, subminiature integrated circuits, microchips, and nanomachines.

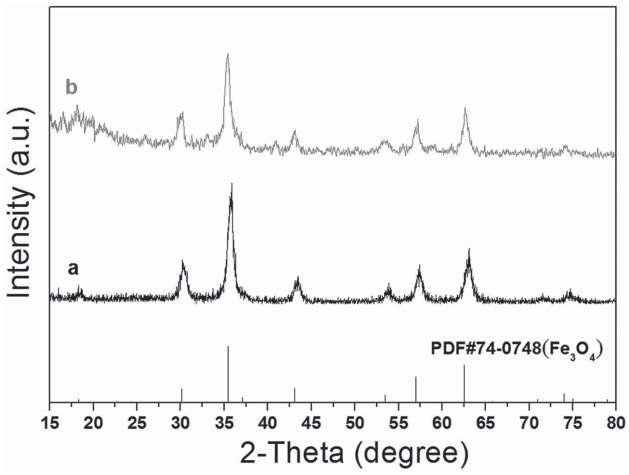

Figure 1. XRD patterns of a) the Fe_3O_4 NPs and b) [Fe_3O_4/PANI/PMMA]//[$Tb(BA)_3$phen/PMMA] Janus nanoribbons array.

2. Results and Discussion

2.1. Phase Analyses

The phase compositions of the Fe_3O_4 NPs and [Fe_3O_4/PANI/PMMA]//[$Tb(BA)_3$phen/PMMA] Janus nanoribbons array were characterized by means of X-ray diffractometry (XRD) analysis, as shown in **Figure 1**. The XRD patterns of the as-prepared Fe_3O_4 NPs conform to the cubic structure of Fe_3O_4 (PDF 74-0748) and no characteristic peaks are observed for other impurities such as Fe_2O_3 and FeO(OH). The XRD analysis results of Janus nanoribbons array demonstrate that the Janus nanoribbons array contains Fe_3O_4 NPs, and the broad diffraction peak extending from 15° to 20° is attributed to the amorphous PMMA and PANI.[29,30]

2.2. Morphology and Internal Structure

The morphology of the as-prepared Fe_3O_4 NPs was observed by means of transmission electron microscopy (TEM), as presented in **Figure 2**a. The size distribution of the spherical Fe_3O_4 NPs is almost uniform and the particle size of the NPs is 9.85 ± 1.60 nm (Figure 2b). The scanning electron microscope (SEM) images of the Janus nanoribbons array were indicated in Figure 2c,d. One can see that almost all the Janus nanoribbons are aligned in the same direction. The width of Janus nanoribbons is 9.51 ± 0.20 μm (Figure 2e), and the thickness of them is 823 ± 1.18 nm (Figure 2f). Moreover, it can be seen that almost all the broadsides of these nanoribbons are facing up, with few exceptions. This is probably because this arrangement helps the nanoribbons lay in a more stable and lower potential energy state onto the aluminum rotary drum. Depending on the transmission light of biological microscope (BM), the inner structures of the Janus nanoribbons can be observed. As revealed in Figure 2g,h, a clear Janus structure can be seen in the Janus nanoribbons. One side of a Janus nanoribbon contains large quantities of dark-colored PANI and Fe_3O_4 NPs, and by contrast, the other side is transparent.

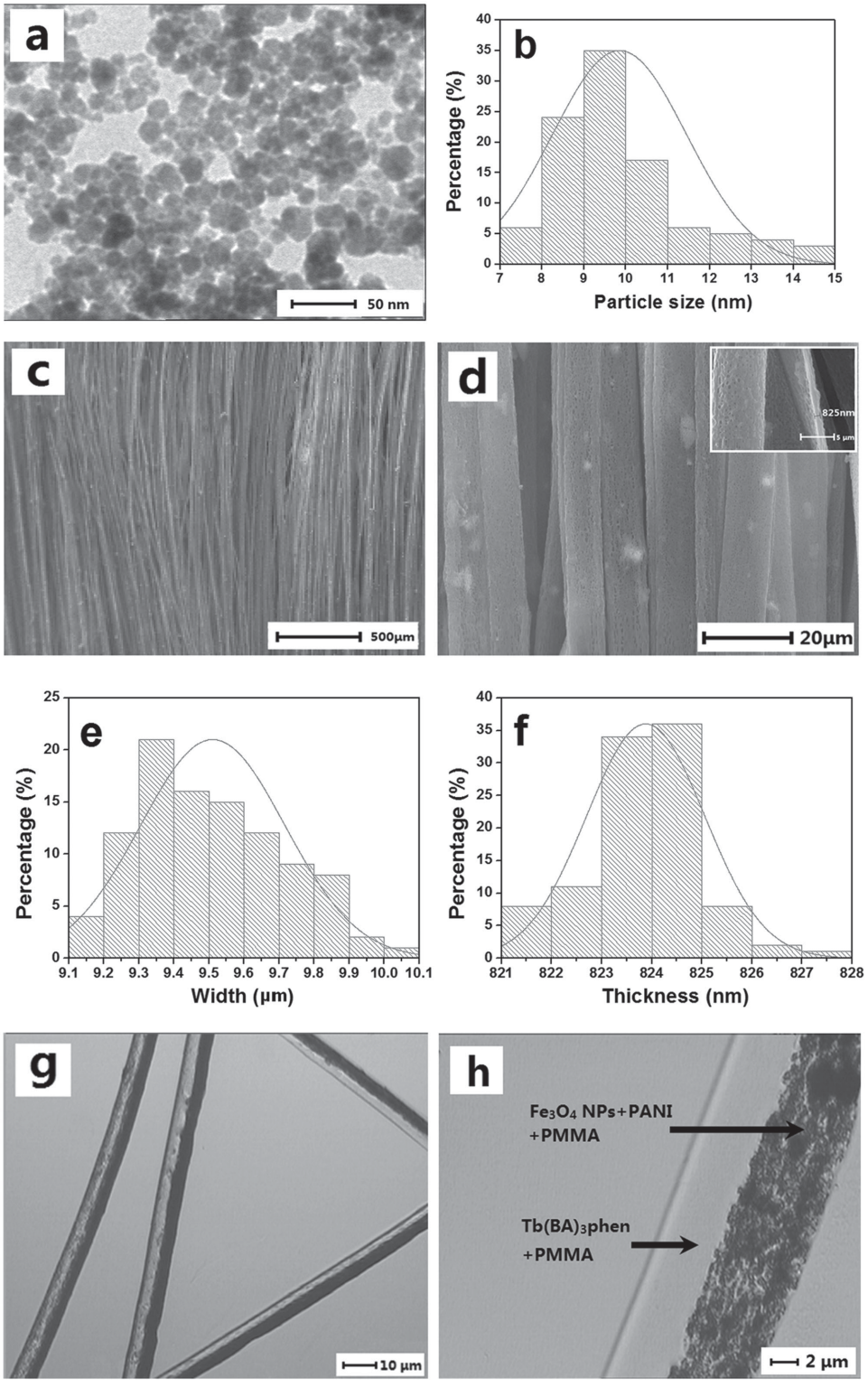

Figure 2. a) TEM image and b) histogram of particle size of Fe_3O_4 NPs; c,d) SEM images, e,f) histograms of width and thickness distribution, and g,h) BM images of [Fe_3O_4/PANI/PMMA]//[Tb(BA)$_3$phen/PMMA] Janus nanoribbons array. The inset of Figure 2d shows the thickness of a Janus nanoribbon.

In order to further investigate the structure of the Janus nanoribbons in the array, energy-dispersive spectroscopy (EDS) line-scan analysis was performed, where S, Fe, and Tb elements represent CSA doped PANI, Fe_3O_4, and Tb(BA)$_3$phen, respectively, as shown in **Figure 3**. Elemental S and Fe only exist in one side of a Janus nanoribbon while elemental Tb only

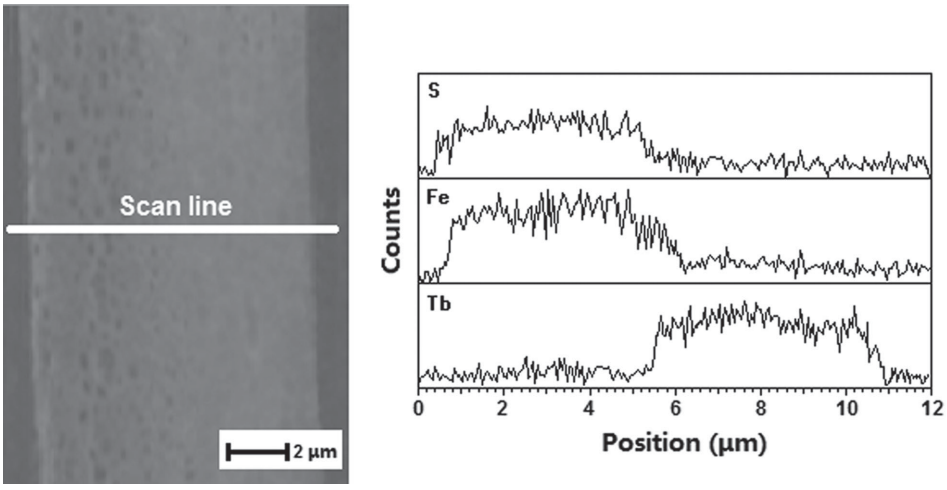

Figure 3. EDS line-scan analysis of a single [Fe_3O_4/PANI/PMMA]//[Tb(BA)$_3$phen/PMMA] Janus nanoribbon in array.

exists in the other side. These results are consistent with asymmetric dual-sided structure of Janus nanoribbons. From the above analyses, we can safely conclude that the [Fe_3O_4/PANI/PMMA]//[Tb(BA)$_3$phen/PMMA] Janus nanoribbons array with a new and interesting nanostructure has been successfully fabricated.

Figure 4 presents the typical digital camera photos of the resulting Janus nanoribbons array. One can see that the Janus nanoribbons array can be freely bent and folded. This is critically important for the application of the material in the flexible device.

2.3. Electrical Conductivity Analysis

For investigating the anisotropic conductivity of the [Fe_3O_4/PANI/PMMA]//[Tb(BA)$_3$phen/PMMA] Janus nanoribbons array, a small piece of soldering tin was cut into four little pieces with diameter of ≈2 mm and was pressed onto the Janus nanoribbons array, as indicated in **Figure 5**a. Then the four pins of a Hall effect measurement system were respectively pressed on the four pieces of soldering tin. The relationships of voltage and current between P1 and P2, P2 and P3, P3 and P4, and P1 and P4 were recorded by the Hall effect measurement system, and the results were presented in Figure 5b. The conductances (G) between P1 and P4, P2 and P3, P1 and P2, and P3 and P4 were calculated by formula: $G = I/U$ and the values were listed in **Table 1**. One can see that the conductance along X direction (P1–P4 and P2–P3) is ≈10^8 higher than that along Y direction (P1–P2 and P3–P4), demonstrating that the Janus nanoribbons array has a strong anisotropy in conductance. To the best of our knowledge, this value, up to now, is the highest conductance ratio of X direction to Y direction.

As described in some literatures,[7,10] anisotropic conductance of an electrospun fibrous membrane can be attributed to the different electrical connection between X and Y directions. Electrons can move without block through the fibers in X direction, whereas a lot of interfaces among the fibers hinder the movement of electrons to some extent in Y direction. However, from the reported anisotropic conductivity results, one can find that the conductivity ratios between X and Y directions of the reported products were very low, meaning that the interfaces cannot effectively hinder the movement of electrons in Y direction. For the Janus nanoribbons array, because each Janus nanoribbon has a insulative-photoluminescent side and almost all the broadsides of the Janus nanoribbons are facing up, the conductive-magnetic sides of the Janus nanoribbons are separated by the plenty of insulative-photoluminescent sides in Y direction (see **Figure 6**), which further blocks the movement of electrons. Therefore, a strong anisotropy in conductivity is achieved in the Janus nanoribbons array.

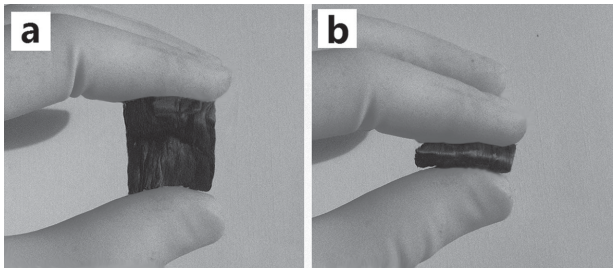

Figure 4. Digital camera photos of the resulting Janus nanoribbons array: a) an unbent Janus nanoribbons array and b) bent Janus nanoribbons array.

2.4. Photoluminescent Property

It has been proven in our previous work that the optimum exciting ultraviolet light for Tb(BA)$_3$phen/PMMA composite materials is 333 nm,[25] thus the 333-nm ultraviolet light was used to excite [Fe_3O_4/PANI/PMMA]//[Tb(BA)$_3$phen/PMMA] Janus nanoribbons array in this work. As seen in **Figure 7**, the Janus nanoribbons array (cut into the size of 5 × 5 cm^2) can emit green light under the excitation of 333-nm ultraviolet light.

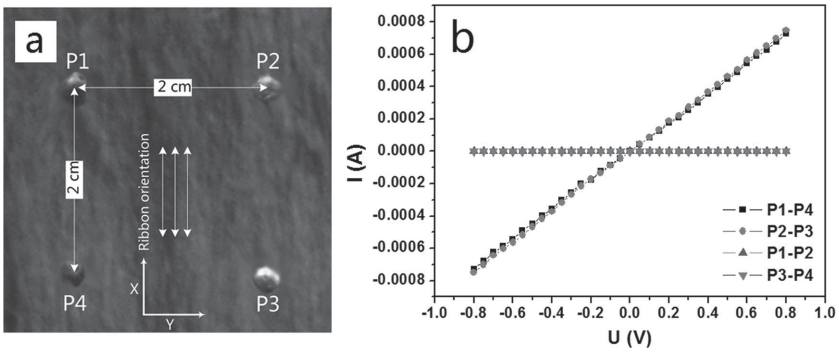

Figure 5. Arrangement of the four contact points on a) [Fe_3O_4/PANI/PMMA]//[Tb(BA)$_3$phen/PMMA] Janus nanoribbons array, and b) relationships of voltage and current between P1 and P2, P2 and P3, P3 and P4, P1 and P4.

Table 1. Conductances between P1 and P4, P2 and P3, P1 and P2, and P3 and P4.

Positions	Conductance [S]
P1–P4	$(8.94 \pm 0.03) \times 10^{-4}$
P2–P3	$(9.27 \pm 0.02) \times 10^{-4}$
P1–P2	$(6.74 \pm 0.02) \times 10^{-12}$
P3–P4	$(7.42 \pm 0.01) \times 10^{-12}$

Figure 8 shows photoluminescence spectra of [Fe_3O_4/PANI/PMMA]//[Tb(BA)$_3$phen/PMMA] Janus nanoribbons array. Characteristic emission peaks of Tb^{3+} are observed under the excitation of 333-nm ultraviolet light and ascribed to the energy levels transitions of $^5D_4 \rightarrow {}^5F_6$ (490 nm), $^5D_4 \rightarrow {}^5F_5$ (545 nm), $^7D_4 \rightarrow {}^5F_4$ (586 nm), and $^5D_4 \rightarrow {}^7F_3$ (622 nm), and the $^5D_4 \rightarrow {}^5F_5$ hypersensitive transition at 545 nm is the predominant emission peak.

2.5. Magnetic Property

The typical hysteresis loop for [Fe_3O_4/PANI/PMMA]//[Tb(BA)$_3$phen/PMMA] Janus nanoribbons array is shown in **Figure 9**. It is well known that the saturation magnetization of a magnetic composite material depends on the mass percentage of the magnetic substance in the magnetic composite material.[25–28] The saturation magnetization of the Janus nanoribbons array is 23.52 emu g^{-1}, and the remanence nears zero, indicating that the Janus nanoribbons array possesses superparamagnetic property.

3. Conclusions

In summary, novel flexible [Fe_3O_4/PANI/PMMA]//[Tb(BA)$_3$phen/PMMA] Janus nanoribbons array with strongly anisotropic conductivity, magnetism and photoluminescence has been successfully fabricated by electrospinning using specially designed parallel spinneret. The array is composed of Janus nanoribbons arranged in the same direction, and all the broadsides of these nanoribbons are facing up. Each Janus nanoribbon in the array consists of a Fe_3O_4/PANI/PMMA conductive-magnetic side and a Tb(BA)$_3$phen/PMMA insulative-photoluminescent side. This unique nanostructure greatly promotes conductive anisotropy, in which the conductance ratio between X and Y directions reaches up to 10^8. The Janus nanoribbons array can emit green light under the excitation of ultraviolet light and has response in the magnetic field. The Janus nanoribbons array resolves many deficiencies of the existing type II ACFs, such as high brittleness, small size, and low conductance ratio between X and Y directions.

4. Experimental Section

Chemicals: Methylmethacrylate (MMA), benzoylperoxide (BPO), Tb_4O_7, benzoic acid (BA), 1,10-phenanthroline (phen), $FeCl_3 \cdot 6H_2O$, $FeSO_4 \cdot 7H_2O$, NH_4NO_3, polyethylene glycol (PEG, Mr ≈ 20 000), ammonia, oleic acid (OA), aniline (ANI), (IS)-(+)-camphor-10 sulfonic acid (CSA), ammonium persulfate (APS), anhydrous ethanol, $CHCl_3$, N,N-dimethylformamide (DMF), and deionized water were used. All the reagents were of analytical grade and were directly used as received without further purification. The purity of Tb_4O_7 was 99.99%. The deionized water was homemade.

Preparation of OA Modified Fe_3O_4 Nanoparticles: Fe_3O_4 nanoparticles (NPs) with the saturation magnetization of 62.02 emu g^{-1} were obtained by using a facile coprecipitation synthetic method,[26] and PEG was used as the protective agent to prevent the particles from aggregation. One typical synthetic procedure was as follows: $FeCl_3 \cdot 6H_2O$ (5.4060 g), $FeSO_4 \cdot 7H_2O$ (2.7800 g), NH_4NO_3 (4.0400 g), and PEG (1.9000 g)

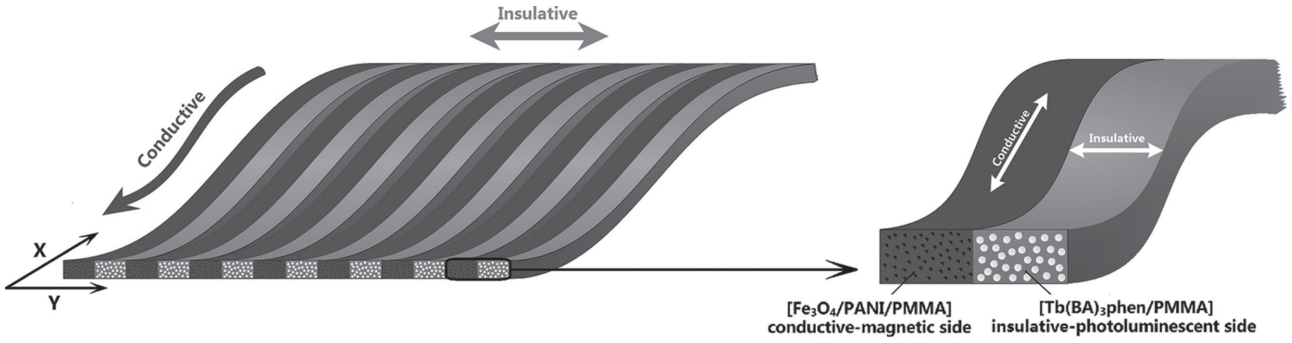

Figure 6. Schematic diagram of electrical property of Janus nanoribbons array.

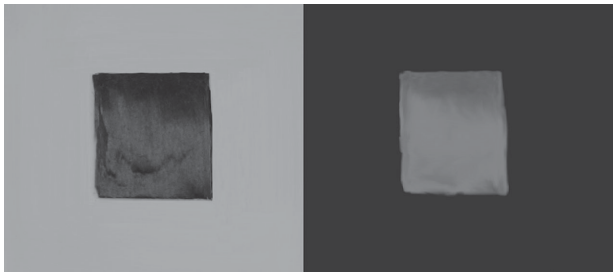

Figure 7. Digital photos of $[Fe_3O_4/PANI/PMMA]//[Tb(BA)_3phen/PMMA]$ Janus nanoribbons array taken in natural light (left) and under the excitation of 333-nm ultraviolet light in the darkness (right).

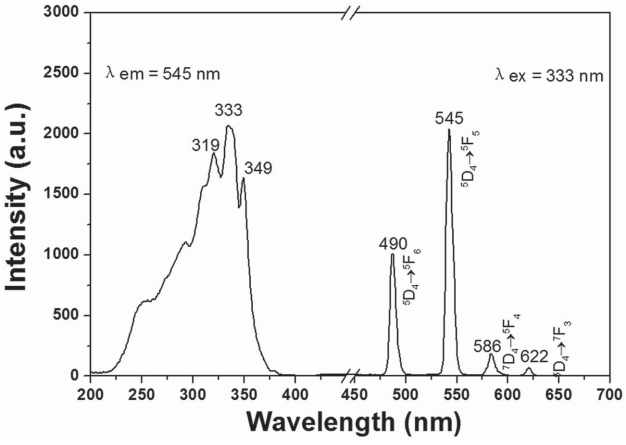

Figure 8. Photoluminescence spectra of $[Fe_3O_4/PANI/PMMA]//[Tb(BA)_3phen/PMMA]$ Janus nanoribbons array.

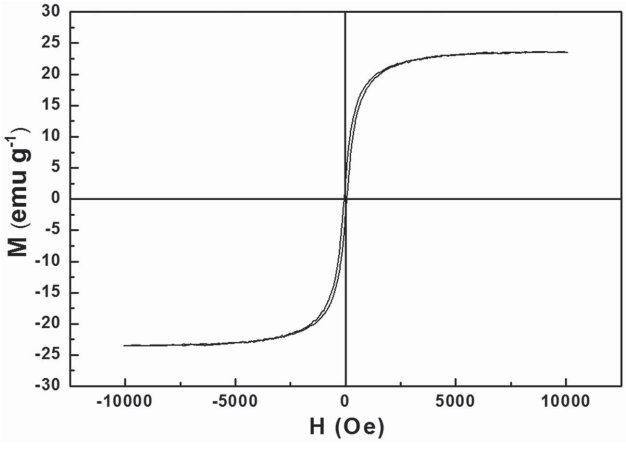

Figure 9. Hysteresis loop for $[Fe_3O_4/PANI/PMMA]//[Tb(BA)_3phen/PMMA]$ Janus nanoribbons array.

were added to deionized water (100 mL) to form a uniform solution under vigorous stirring at 50 °C. To prevent the oxidation of Fe^{2+}, the reactive mixture was kept under an argon atmosphere. After the mixture had been bubbled with argon for 30 min, $NH_3{\cdot}H_2O$ (0.1 mol L^{-1}) was dropwise added into the mixture until the pH value was above 11. Then the system was continuously bubbled with argon for 20 min at 50 °C and black precipitates were formed. The precipitates were collected from the solution by magnetic separation, washed with deionized water for three times, and then dried in an electric vacuum oven for 12 h at 60 °C. To improve the monodispersity, stability, and solubility of Fe_3O_4 NPs in the spinning solution, the as-prepared Fe_3O_4 NPs were coated with OA as below: the as-prepared Fe_3O_4 NPs (1.5000 g) were ultrasonically dispersed in deionized water (50 mL) for 20 min. The suspension was heated to 80 °C under an argon atmosphere with vigorous mechanical stirring for 30 min and then OA (0.5 mL) was slowly added. The reaction was stopped after heating and stirring the mixture for 40 min. The precipitates were collected from the solution by magnetic separation, washed with ethyl alcohol for three times, and then dried in an electric vacuum oven at 60 °C for 6 h. Then, all of the products were used to prepare spinning solution I.

Synthesis of $Tb(BA)_3phen$ Complexes: $Tb(BA)_3phen$ powders were synthesized according to the traditional method as described in the literature.[27] Tb_4O_7 (1.8693 g) was dissolved in concentrated nitric acid (10 mL) and then crystallized via evaporation of the excess amount of nitric acid and water by heating and $Tb(NO_3)_3{\cdot}6H_2O$ was acquired. An ethanol solution of $Tb(NO_3)_3$ was prepared by adding anhydrous ethanol (10 mL) to the above $Tb(NO_3)_3{\cdot}6H_2O$. BA (1.8320 g) and phen (0.9910 g) were dissolved in ethanol (100 mL). The $Tb(NO_3)_3$ solution was then added into the mixture solution of BA and phen with magnetic agitation for 3 h at 60 °C. The precipitate was collected by filtration and dried for 12 h at 60 °C.

Preparation of PMMA: PMMA used in this study was prepared by oxidative polymerization of MMA according to ref. [28]. MMA (100 mL) and BPO (0.1000 g) were mixed in a 250-mL three-necked flask with a backflow device and vigorously stirred at 90–95 °C. When the viscosity of the solution reached a certain value just like that of glycerol, the heating was stopped and it was left to naturally cool down to room temperature. The obtained gelatinous solution was then loaded into test tubes, and the influx height was 5–7 cm. After that, the tubes were put in an electric vacuum oven for 48 h at 50 °C, and the gelatinous solution was then solidified. Finally, the temperature in the oven was raised to 110 °C for 2 h to terminate the reaction.

Preparation of Spinning Solutions for Fabricating $[Fe_3O_4/PANI/PMMA]//[Tb(BA)_3phen/PMMA]$ Janus Nanoribbons Array: Two different kinds of spinning solutions were prepared to fabricate Janus nanoribbons array. The spinning solution for the conductive-magnetic side of the Janus nanoribbons in the array was composed of CSA doped PANI, OA modified Fe_3O_4 NPs, PMMA, $CHCl_3$, and DMF (denoted as spinning solution I). In the preparation of spinning solution I, 0.5000 g of PMMA was dissolved into the mixed solution of $CHCl_3$ (9.3750 g) and DMF (0.6250 g) under magnetic stirring for 48 h. The mixture was then cooled down to 0 °C in an ice-bath. In order to find the optimum of adding dosage of ANI, various amounts of ANI and CSA were added into the above mixture and kept stirring for 2 h, followed by introducing APS and stirring for 30 min. The final mixture was allowed to react at 0 °C for 24 h and then the as-prepared OA modified Fe_3O_4 NPs were added into the mixture under mechanical stirring for 2 h at room temperature, thus the spinning solution I was prepared. For performing the electrical conductivity tests, 2 mL of the spinning solution I was dripped onto a piece of glass and the solvent was allowed to volatilize at room temperature for 48 h. The dosages of ANI, CSA, APS, and the corresponding conductivities were shown in **Table 2**. One can see that

Table 2. Dosages of ANI, CSA, APS, and corresponding conductivities.

ANI [g]	CSA [g]	APS [g]	Conductivity [S cm^{-1}]
0.0500	0.0625	0.1225	1.974×10^{-6}
0.1000	0.1249	0.2450	3.931×10^{-4}
0.1500	0.1873	0.3676	1.092×10^{-2}
0.2000	0.2497	0.4900	1.475×10^{-2}
0.2500	0.3125	0.6125	1.874×10^{-2}

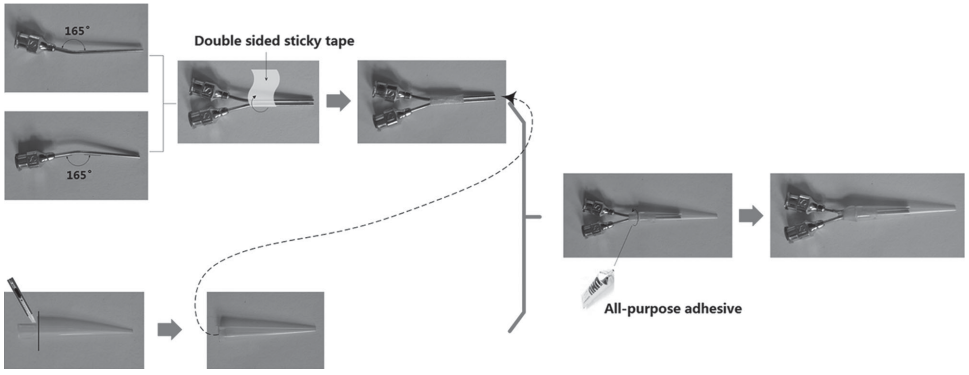

Figure 10. Schematic diagram of manufacturing process for parallel spinneret.

the conductivity can reach up to the order of 10^{-2} S cm^{-1} and it increases not much with adding more ANI than 0.1500 g. Thus the spinning solution I containing 0.1500 g ANI was adopted for the subsequent study. The other spinning solution for the insulative-photoluminescent side consisted of $Tb(BA)_3$phen, PMMA, $CHCl_3$, and DMF (denoted as spinning solution II). It has been known through our previous work that the optimum ratio of $Tb(BA)_3$phen to PMMA is 1:10.[25] Thus for the preparation of the spinning solution II, PMMA (0.5000 g) and $Tb(BA)_3$phen (0.0500 g) were added into the mixed solution of $CHCl_3$ (9.3750 g) and DMF (0.6250 g) under magnetic stirring for 48 h.

Electrospinning Equipment for Fabricating [Fe_3O_4/PANI/PMMA]// [$Tb(BA)_3$phen/PMMA] Janus Nanoribbons Array: A specially designed parallel spinneret was used for fabricating the Janus nanoribbons array. The manufacturing process of the parallel spinneret is shown in **Figure 10**. Two truncated 12 # stainless steel needles (inner/outer diameter: 0.90/1.26 mm) were bended at a certain angle and assembled side by side with double sided sticky tape. A plastic nozzle was cut to an appropriate length and put on over the tip of the pair of stainless steel needles. At last, an all-purpose adhesive was used to seal the space between the pair of stainless steel needles and the cut section of plastic nozzle. The equipment for the electrospinning process is presented in **Figure 11**. The spinning solution I and spinning solution II were separately loaded into the two plastic syringes. In order to obtain Janus nanoribbons array, an aluminum rotary drum was used as a nanoribbons collector, which was put about 18 cm away from the tip of the plastic nozzle. The aluminum rotary drum was 20 cm in length, 7 cm in diameter, fixed in horizontal, and the rotation speed was 1500 r min^{-1}. A positive direct current voltage of 6 kV was applied between the spinneret and the collector to generate stable, continuous PMMA-based Janus nanoribbons array at room temperature of 20–22 °C and the relative humidity of 20%–30%. In the electrospinning process, the two spinning solutions at the tip of the plastic nozzle have formed a side-by-side structure, and they are then stretched by electric field force to form a Janus Tylor cone and a Janus jet. The Janus jet is stretched to ribbon shape by electrostatic repulsion and solidified with the volatilization of solvents, thus a Janus nanoribbon is obtained. Furthermore, because the Janus nanoribbon swings in the air due to the instability of electrospinning process, an array with a certain width can be collected on the surface of the aluminum rotary drum.

Characterization: The phase compositions were identified by an X-ray powder diffractometer (Bruker, D8 FOCUS) with CuKα radiation. The operation voltage and current were kept at 40 kV and 20 mA, respectively. The morphologies and internal structures were observed by a field-emission SEM (FESEM, XL-30), a transmission electron microscope (TEM, JEM-2010), and a biological microscope (BM, CVM500E). The elemental analysis was performed by an energy-dispersive spectrometer (Oxford Instruments) attached to the FESEM. The electrical properties were measured by a Hall effect measurement system (ECOPIA HMS-3000). The fluorescent properties were investigated by Hitachi fluorescence spectrophotometer F-7000. The UV–vis absorption spectra were recorded by a UV–vis spectrophotometer (SHIMADZU UV mini 1240). Then, the magnetic performances were measured by a vibrating

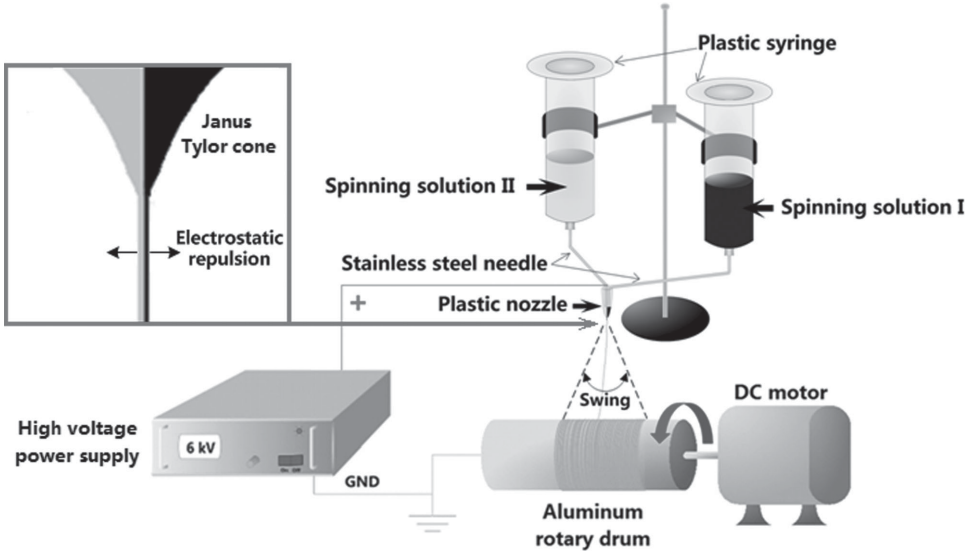

Figure 11. Schematic diagram of electrospinning equipment for preparing a Janus nanoribbons array.

sample magnetometer (MPMS SQUID XL). All the determinations were performed at room temperature.

Acknowledgements

This work was financially supported by the National Natural Science Foundation of China (NSFC 50972020 and 51072026), Specialized Research Fund for the Doctoral Program of Higher Education (20102216110002 and 20112216120003), the Science and Technology Development Planning Project of Jilin Province (Grant Nos. 20130101001JC, 20070402, and 20060504), the Science and Technology Research Project of the Education Department of Jilin Province during the eleventh five-year plan period (Under Grant No. 2010JYT01).

Received: January 27, 2015
Revised: February 14, 2015
Published online: March 12, 2015

[1] C. M. Lin, W. J. Chang, T. H. Fang, *IEEE Trans. Device Mater. Reliab.* **2005**, *5*, 694.
[2] I. Kim, K. W. Paik, *J. Electron. Mater.* **2014**, *43*, 3236.
[3] D. H. Baek, J. S. Park, E. J. Lee, S. J. Shin, J. H. Moon, J. J. Pak, S. H. Lee, *IEEE Trans. Biomed. Eng.* **2011**, *58*, 1466.
[4] S. Asai, U. Saruta, M. Tobita, M. Takano, Y. Miyashita, *J. Appl. Polym. Sci.* **1995**, *56*, 769.
[5] D. D. Lu, C. P. Wong, *Adv. Flip Chip Packag.* **2013**, 201.
[6] B. Li, H. Y. Jung, H. L. Wang, Y. L. Kim, T. Kim, H. G. Hahm, A. Busnaina, M. Upmanyu, Y. J. Jung, *Adv. Funct. Mater.* **2011**, *21*, 1810.
[7] Z. P. Zhou, C. L. Lai, L. F. Zhang, Y. Qian, H. Q. Hou, F. H. Reneker, H. Fong, *Polymer* **2009**, *50*, 2999.
[8] F. Greco, T. Fujie, L. Ricotti, S. Taccola, B. Mazzolai, V. Mattoli, *ACS Appl. Mater. Interfaces* **2013**, *5*, 573.
[9] T. I. Jeon, K. J. Kim, C. Kang, I. H. Maeng, J. H. Son, K. H. An, J. Y. Lee, Y. H. Lee, *J. Appl. Phys.* **2004**, *95*, 5736.
[10] E. J. Ra, K. H. An, K. K. Kim, S. Y. Jeong, Y. H. Lee, *Chem. Phys. Lett.* **2005**, *413*, 188.
[11] P. W. Majewski, M. Gopinadhan, W. S. Jang, J. L. Lutkenhaus, C. O. Osuji, *J. Am. Chem. Soc.* **2010**, *132*, 17516.
[12] J. R. Huang, Y. T. Zhu, W. Jiang, J. H. Yin, Q. X. Tang, X. D. Yang, *ACS Appl. Mater. Interfaces* **2014**, *6*, 1754.
[13] W. Sambaer, M. Zatloukal, D. Kimmer, *Chem. Eng. Sci.* **2011**, *66*, 613.
[14] J. M. Corres, Y. R. Garcia, F. J. Arregui, I. R. Matias, *IEEE Sens. J.* **2011**, *11*, 2383.
[15] A. Townsend-Nicholson, S. N. Jayasinghe, *Biomacromolecules* **2006**, *7*, 3364.
[16] Y. J. Zhu, X. G. Han, Y. H. Xu, Y. H. Liu, S. Y. Zheng, K. Xu, L. B. Hu, *ACS Nano* **2013**, *7*, 6378.
[17] Z. Y. Hou, C. X. Li, P. A. Ma, G. G. Li, Z. Y. Cheng, C. Peng, D. M. Yang, P. P. Yang, J. Lin, *Adv. Funct. Mater.* **2011**, *21*, 2356.
[18] M. Y. Zhang, C. L. Shao, J. B. Mu, X. M. Huang, Z. Y. Zhang, Z. C. Guo, P. Zhang, Y. C. Liu, *J. Mater. Chem.* **2012**, *22*, 577.
[19] M. Y. Zhang, C. L. Shao, X. H. Li, P. Zhang, Y. Y. Sun, C. Y. Su, X. Zhang, J. J. Ren, Y. C. Liu, *Nanoscale* **2012**, *23*, 7501.
[20] D. Li, Y. L. Wang, Y. N. Xia, *Nano Lett.* **2003**, *3*, 1167.
[21] D. V. Isakov, E. de M. Gomes, L. G. Vieira, T. Dekola, M. S. Belsley, B. G. Almeida, *ACS Nano* **2011**, *5*, 73.
[22] L. Gu, N. Y. Cui, L. Cheng, Q. Xu, S. Bai, M. M. Yuan, W. W. Wu, J. M. Liu, Y. Zhao, F. Ma, Y. Qin, Z. L. Wang, *Nano Lett.* **2013**, *13*, 91.
[23] G. Morello, M. Moffa, S. Girardo, A. Camposeo, D. Pisignano, *Adv. Funct. Mater.* **2014**, *24*, 5225.
[24] Z. Sun, J. M. Deitzel, J. Knopf, X. Chen, J. W. Gillespie, *J. Appl. Polym. Sci.* **2012**, *152*, 2585.
[25] Q. L. Ma, W. S. Yu, X. T. Dong, J. X. Wang, G. X. Liu, *Nanoscale* **2014**, *6*, 2945.
[26] Q. L. Ma, J. X. Wang, X. T. Dong, W. S. Yu, G. X. Liu, J. Xu, *J. Mater. Chem.* **2012**, *22*, 14438.
[27] Q. L. Ma, J. X. Wang, X. T. Dong, W. S. Yu, G. X. Liu, *ChemPlusChem* **2014**, *79*, 290.
[28] Q. L. Ma, W. S. Yu, X. T. Dong, J. X. Wang, G. X. Liu, J. Xu, *Opt. Mater.* **2013**, *35*, 526.
[29] A. K. Tomar, S. Mahendia, S. Kumar, *Adv. Appl. Sci. Res.* **2011**, *2*, 327.
[30] S. Ray, A. J. Easteal, R. P. Cooney, N. R. Edmonds, *Mater. Chem. Phys.* **2009**, *113*, 829.